

Insights and challenges of applying the *GW* method to transition metal oxides

Georgy Samsonidze,¹ Cheol-Hwan Park,² and Boris Kozinsky¹

¹*Research and Technology Center, Robert Bosch LLC, Cambridge, Massachusetts 02142, USA*

²*Department of Physics, Seoul National University, Seoul 151-747, Korea*

(Dated: October 31, 2014)

The *ab initio* *GW* method is considered as the most accurate approach for calculating the band gaps of semiconductors and insulators. Yet its application to transition metal oxides (TMOs) has been hindered by the failure of traditional approximations developed for conventional semiconductors. In this work, we examine the effects of these approximations on the values of band gaps for ZnO, Cu₂O, and TiO₂. In particular, we explore the origin of the differences between the two widely used plasmon-pole models. Based on the comparison of our results with the experimental data and previously published calculations, we discuss which approximations are suitable for TMOs and why.

This is an author-created, un-copyedited version of an article published in Journal of Physics: Condensed Matter. IOP Publishing Ltd is not responsible for any errors or omissions in this version of the manuscript or any version derived from it. The Version of Record is available online at doi:10.1088/0953-8984/26/47/475501.

I. INTRODUCTION

Many-body perturbation theory within the *GW* approximation has been successfully used to describe the electronic spectra of *sp*-bonded semiconductors and insulators from first principles [1–10]. However, application of the *GW* methodology to materials with localized *d*-electrons, such as transition metal oxides (TMOs), has revealed some controversial results. One of the heavily debated topics is the *GW* band gap of ZnO for which values ranging from 2.1 to 3.9 eV have been reported [11–27]. This wide variation can be attributed to the use of different self-consistent schemes [12–14, 16, 28, 29], plasmon-pole models (PPMs) [21, 23, 26], and starting points [15, 17, 20], as well as to a false convergence behavior as discussed in Ref. 17 and to the basis set convergence issues as discussed in Refs. 18 and 27. At the same time, it is difficult to pinpoint the contributions of each approximation (self-consistent scheme, PPM, and starting point) to the total difference, since the different results reported in the literature were obtained with different codes and with different sets of numerical parameters.

The motivation behind the present study was to systematically isolate the contributions of these approximations. For that purpose we performed multiple *GW* calculations for three TMOs (wurtzite ZnO, cuprite Cu₂O, and rutile TiO₂) using many possible combinations of these approximations. Analyzing the results of these calculations allowed us to collect valuable information about the validity and applicability of these approximations. We were able to show that the theoretically justified choice of approximations gives the best agreement with experiment for all the materials studied. We further discuss the origin of the differences between the two widely used PPMs, and we demonstrate how one of them can be modified to give better accuracy as compared to the results of higher level calculations.

The paper is organized as follows. Sec. II gives the theoretical background, followed by the computational details in Sec. III. Sec. IV presents the results and a discussion thereof. The main findings of this work are summarized in Sec. V.

II. THEORETICAL BACKGROUND

Within the *GW* approximation, the electron self-energy operator Σ is given by [1, 7, 9, 10, 30, 31]:

$$\Sigma(\mathbf{r}, \mathbf{r}'; \omega) = \frac{i}{2\pi} \int d\omega' e^{i\omega'\eta} \times G(\mathbf{r}, \mathbf{r}'; \omega + \omega') W(\mathbf{r}, \mathbf{r}'; \omega') \quad (1)$$

where \mathbf{r} is the spatial coordinate, ω is the energy, η is a positive infinitesimal, G is the Green's function, and W is the screened Coulomb potential. The expression for G is:

$$G(\mathbf{r}, \mathbf{r}'; \omega) = \sum_{n\mathbf{k}} \frac{\psi_{n\mathbf{k}}^{\text{QP}}(\mathbf{r}) \psi_{n\mathbf{k}}^{\text{QP}*}(\mathbf{r}')}{\omega - E_{n\mathbf{k}}^{\text{QP}} - i\eta_{n\mathbf{k}}} \quad (2)$$

where n is the band index, \mathbf{k} is the Bloch wave vector, $\psi_{n\mathbf{k}}^{\text{QP}}(\mathbf{r})$ is the quasiparticle orbital, $E_{n\mathbf{k}}^{\text{QP}}$ is the quasiparticle energy, and $\eta_{n\mathbf{k}}$ is a positive (negative) infinitesimal for occupied (unoccupied) states. The expression for W is:

$$W(\mathbf{r}, \mathbf{r}'; \omega) = \int d\mathbf{r}'' \epsilon^{-1}(\mathbf{r}, \mathbf{r}''; \omega) v(\mathbf{r}'' - \mathbf{r}') \quad (3)$$

where ϵ is the microscopic dielectric function, $v(\mathbf{r}) = e^2/|\mathbf{r}|$ is the bare Coulomb potential, and e is an elementary charge. The expression for ϵ is:

$$\epsilon(\mathbf{r}, \mathbf{r}'; \omega) = \delta(\mathbf{r} - \mathbf{r}') - \int d\mathbf{r}'' v(\mathbf{r} - \mathbf{r}'') P(\mathbf{r}'', \mathbf{r}'; \omega) \quad (4)$$

where δ is the Dirac delta function and P is the polarizability. The latter is evaluated within the random phase approximation (RPA):

$$P(\mathbf{r}, \mathbf{r}'; \omega) = -\frac{i}{2\pi} \int d\omega' G(\mathbf{r}, \mathbf{r}'; \omega + \omega') G(\mathbf{r}', \mathbf{r}; \omega') \quad (5)$$

Calculations are performed in reciprocal space, for instance $\epsilon(\mathbf{r}, \mathbf{r}'; \omega)$ is Fourier transformed to $\epsilon_{\mathbf{G}\mathbf{G}'}(\mathbf{q}; \omega)$, where \mathbf{G} is the reciprocal lattice vector and \mathbf{q} is the Bloch wave vector.

In practice, the GW method is applied perturbatively on top of Kohn-Sham density functional theory (DFT) [32] calculations. It is often assumed that the Kohn-Sham orbitals $\psi_{n\mathbf{k}}^{\text{KS}}(\mathbf{r})$ are good approximation for the quasiparticle orbitals $\psi_{n\mathbf{k}}^{\text{QP}}(\mathbf{r})$. Σ is then diagonal in the basis of $\psi_{n\mathbf{k}}^{\text{KS}}$ and the quasiparticle energies are expressed by [7]:

$$E_{n\mathbf{k}}^{\text{QP}} = E_{n\mathbf{k}}^{\text{KS}} + \langle \psi_{n\mathbf{k}}^{\text{KS}}(\mathbf{r}) | \Sigma(\mathbf{r}, \mathbf{r}'; E_{n\mathbf{k}}^{\text{QP}}) - V_{\text{xc}}[\rho_{\text{scf}}(\mathbf{r})](\mathbf{r})\delta(\mathbf{r} - \mathbf{r}') | \psi_{n\mathbf{k}}^{\text{KS}}(\mathbf{r}') \rangle \quad (6)$$

where $E_{n\mathbf{k}}^{\text{KS}}$ are the Kohn-Sham energies, V_{xc} is the exchange-correlation potential, and ρ_{scf} is the self-consistent charge density.

The Kohn-Sham ansatz is often used in conjunction with *ab initio* pseudopotentials [33] assuming separation of electrons into core and valence states. This implies that the Σ and V_{xc} terms of Eq. (6) only include contributions from the valence states, while contributions from the core states are treated at the DFT level in the $E_{n\mathbf{k}}^{\text{KS}}$ term of Eq. (6), and the core-valence interaction is neglected [2, 7]. The latter is of particular concern when core and valence orbitals overlap, such as would occur in Zn if $1s^2 2s^2 2p^6 3s^2 3p^6$ states were treated as core states and $3d^{10} 4s^2$ states as valence states. The core-valence interaction can be included at the DFT level using the non-linear core correction (NLCC) [34] which introduces the partial core charge density ρ_{core} in the evaluation of the exchange-correlation potential, $V_{\text{xc}}[\rho_{\text{core}} + \rho_{\text{scf}}]$. The GW method on the other hand requires the entire shell of semicore states (such as $3s^2 3p^6 3d^{10}$ states in Zn) to be explicitly treated as valence states in order to eliminate errors due to neglecting the core-valence interaction [35–39]. All calculations in this work are performed treating the entire third shells of Zn, Cu, and Ti as valence states.

The core-valence partitioning brings up another issue, namely that the charge density used for the evaluation of the V_{xc} term in Eq. (6) must be consistent with the orbitals used in the construction of the Σ operator in the said equation [31, 40–42]. In particular, it was shown that if the NLCC is used in the DFT calculation, ρ_{core} must be set to zero when evaluating the V_{xc} term of Eq. (6) [41]. To study the effect of imbalance between the Σ and V_{xc} terms in Eq. (6), we use ρ_{core} derived from the deep core states (such as $2s^2 2p^6$ states in Zn). Even though there is negligible overlap between the deep core and semicore orbitals (such as the second and third shells of Zn), the integrated partial core charge $q_{\text{core}} = \int d\mathbf{r} \rho_{\text{core}}(\mathbf{r})$ is not

small ($q_{\text{core}} = 7.67e$ in Zn). In what follows we examine how keeping ρ_{core} in the V_{xc} term of Eq. (6) affects the results of GW calculations as compared to the case of zeroing out ρ_{core} in the V_{xc} term.

Several different approaches have been developed for constructing Σ and calculating its matrix elements entering Eq. (6):

- Non-self-consistent G_0W_0 scheme [7] when G and P are obtained by plugging $\psi_{n\mathbf{k}}^{\text{KS}}$ and $E_{n\mathbf{k}}^{\text{KS}}$ into Eqs. (2) and (5).
- Eigenvalue self-consistent GW scheme [13] when G and P are constructed from $\psi_{n\mathbf{k}}^{\text{KS}}$ and $E_{n\mathbf{k}}^{\text{QP}}$, the latter being determined iteratively starting from $E_{n\mathbf{k}}^{\text{KS}}$.
- Eigenvalue self-consistent GW_0 scheme [13] when G is calculated using $\psi_{n\mathbf{k}}^{\text{KS}}$ and $E_{n\mathbf{k}}^{\text{QP}}$ while P is calculated using $\psi_{n\mathbf{k}}^{\text{KS}}$ and $E_{n\mathbf{k}}^{\text{KS}}$.
- Eigenvector self-consistent GW schemes [28, 29, 43] when $\psi_{n\mathbf{k}}^{\text{QP}}$ are constructed iteratively using off-diagonal matrix elements of Σ in the basis of $\psi_{n\mathbf{k}}^{\text{KS}}$.

It was shown that the self-consistent GW scheme without the vertex correction in Σ (beyond the GW approximation) overestimates the experimental band gaps [44]. Better agreement with experiment is obtained using the GW_0 scheme because the effects of self-consistency in W and of vertex correction in Σ largely cancel out [45–47]. It should be noted that the self-consistency in G without the vertex correction in Σ violates the Ward-Takahashi identity representing the local electron number conservation law [48]. For the purpose of this work, we employ non-self-consistent G_0W_0 and eigenvalue self-consistent GW_0 schemes.

The energy integral in Eq. (1) can be evaluated by direct numerical integration [30], employing the Hilbert transform [49], the contour deformation technique [50], or using a plasmon-pole model (PPM) to approximate the ω dependence of ϵ^{-1} . The first three methods are thereafter referred as non-PPM. Two popular choices for PPM are the Hybertsen-Louie (HL) PPM [7, 51] and the Godby-Needs (GN) PPM [52]. The HL PPM takes as input the static inverse dielectric function ϵ^{-1} at $\omega = 0$ and the charge density ρ_{ppm} which is used to compute the effective bare plasma frequencies. The GN PPM takes as input ϵ^{-1} at two frequencies, $\omega = 0$ and $\omega = i\Omega$, where Ω is a parameter. The HL PPM recently came under criticism for poorly reproducing the ω dependence of the RPA ϵ^{-1} as compared to the GN PPM [21, 23, 26].

As we show in this paper, the poor performance of the HL PPM stems from the improper choice of ρ_{ppm} . One sensible choice for ρ_{ppm} is the charge density of the valence electrons (oxygen $2p^6$ states), $\rho_{\text{ppm}} = \rho_{\text{val}}$, owing to the fact that the dielectric screening is dominated by the valence electrons [53]. This choice for ρ_{ppm} was implicitly assumed in the original derivation of the HL PPM [7]. Another common choice for ρ_{ppm} is the self-consistent charge density, $\rho_{\text{ppm}} = \rho_{\text{scf}}$, which includes

TABLE I. Pseudopotential parameters for Zn^{2+} , Cu^{2+} , Ti^{2+} , and O. Shown are the electronic core and valence configurations, the integrated partial core charge $q_{\text{core}} = \int d\mathbf{r} \rho_{\text{core}}(\mathbf{r})$, the partial core radius r_{core} determined by the condition $\rho_{\text{core}}(r_{\text{core}}) = 2\rho_{\text{val}}(r_{\text{core}})$, and the matching radii for different angular momentum channels $r_{s,p,d}$. Core charge is in units of elementary charge, all radii are in Bohr.

	Core	Valence	q_{core}	r_{core}	r_s	r_p	r_d
Zn^{2+}	$1s^2 2s^2 2p^6$	$3s^2 3p^6 3d^{10}$	7.67	0.31	1.00	1.00	0.85
Cu^{2+}	$1s^2 2s^2 2p^6$	$3s^2 3p^6 3d^9$	7.53	0.33	1.05	1.05	0.90
Ti^{2+}	$1s^2 2s^2 2p^6$	$3s^2 3p^6 3d^2$	6.27	0.52	1.20	1.25	1.35
O	$1s^2$	$2s^2 2p^4$	1.37	0.34	1.10	1.10	

TABLE II. Parameters of DFT and GW calculations for wurtzite ZnO, cuprite Cu_2O , and rutile TiO_2 . MP stands for a Monkhorst-Pack grid [54] for summing over the Brillouin zone to obtain ρ_{scf} , ρ_{val} , ϵ , and Σ . E_ψ , E_v , E_ϵ , and E_W are kinetic energy cutoffs for the plane wave expansion of $\psi_{n\mathbf{k}}^{\text{KS}}$, v , ϵ , and W , respectively. N_{KS} is the number of Kohn-Sham bands (both occupied and unoccupied) with the energies up to about E_{KS} above the average ($\mathbf{G} = \mathbf{0}$ component) electrostatic (ionic plus Hartree) potential.

	Wurtzite ZnO	Cuprite Cu_2O	Rutile TiO_2
MP $\rho_{\text{scf, val}}$	$9 \times 9 \times 5$	$7 \times 7 \times 7$	$6 \times 6 \times 9$
MP ϵ, Σ	$5 \times 5 \times 3$	$4 \times 4 \times 4$	$3 \times 3 \times 5$
$E_{\psi, v}$ (Ry)	400	350	250
$E_{\epsilon, W}$ (Ry)	80	80	80
N_{KS}	1500	2400	1900
E_{KS} (Ry)	40	40	40

the core electrons treated as valence in the construction of the pseudopotentials (oxygen $2s^2$ states and the transition metal third shell). Our calculations demonstrate that the HL PPM approaches the GN PPM and the RPA results when ρ_{ppm} is set to ρ_{val} . At the same time, the poor performance of the HL PPM discussed in the literature [21, 23, 26] is attributed to setting ρ_{ppm} equal to ρ_{scf} .

TABLE III. Structural parameters of wurtzite ZnO, cuprite Cu_2O , and rutile TiO_2 measured by X-ray diffraction [55–57] and calculated using DFT with LDA and GGA exchange-correlation functionals.

	Wurtzite ZnO			Cuprite Cu ₂ O	Rutile TiO ₂		
	<i>a</i> (Å)	<i>c</i> (Å)	<i>u</i>	<i>a</i> (Å)	<i>a</i> (Å)	<i>c</i> (Å)	<i>u</i>
X-ray ^a	3.25	5.20	0.382	4.27	4.59	2.96	0.305
LDA	3.19	5.16	0.378	4.18	4.56	2.92	0.304
GGA	3.28	5.30	0.379	4.31	4.65	2.97	0.305

^a From Refs. 55–57.

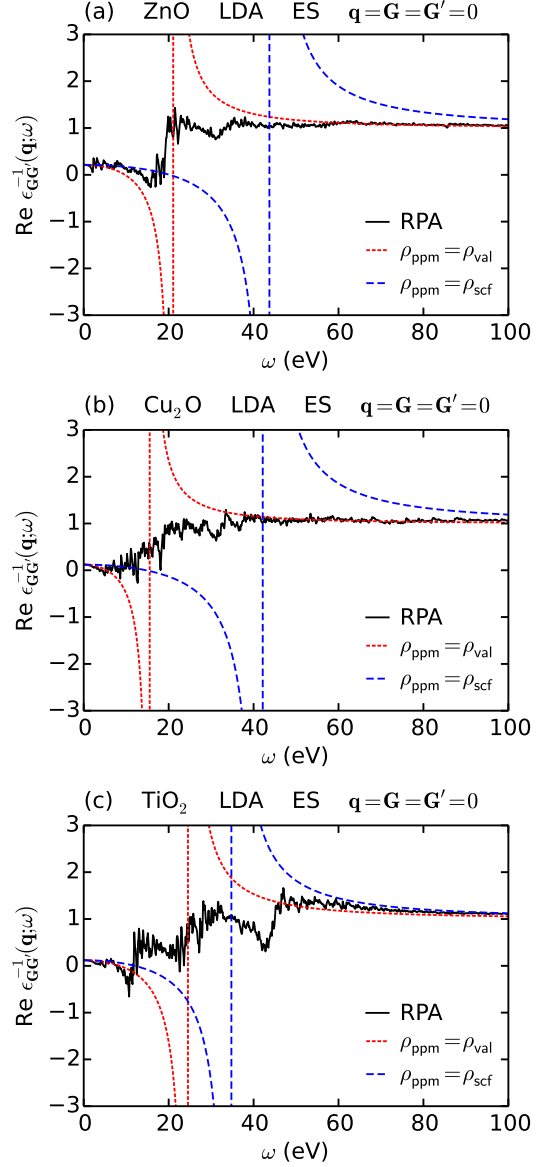


FIG. 1. Real parts of inverse dielectric functions $\epsilon_{\mathbf{GG}'}^{-1}(\mathbf{q}; \omega)$ at $\mathbf{q} = \mathbf{G} = \mathbf{G}' = \mathbf{0}$ of (a) wurtzite ZnO, (b) cuprite Cu_2O , and (c) rutile TiO_2 in case of the LDA starting point and experimental structural parameters (ES) calculated within the RPA (solid black) and constructed using the HL PPM with $\rho_{\text{ppm}} = \rho_{\text{val}}$ (short-dashed red) and $\rho_{\text{ppm}} = \rho_{\text{scf}}$ (long-dashed blue). The HL PPM mode frequencies $\tilde{\omega}_{\mathbf{GG}'}(\mathbf{q})$ are shown by the vertical dashed lines at (a) 21.0 eV and 43.8 eV, (b) 15.6 eV and 42.1 eV, and (c) 24.6 eV and 34.7 eV.

III. COMPUTATIONAL DETAILS

To examine the effects of different approximations discussed in Sec. II on the quasiparticle band gaps and band edges of TMOs, we perform a series of calculations for wurtzite ZnO, cuprite Cu_2O , and rutile TiO_2 using Quantum ESPRESSO [59] and BerkeleyGW [30] codes for the DFT and GW parts, respectively. Calculations

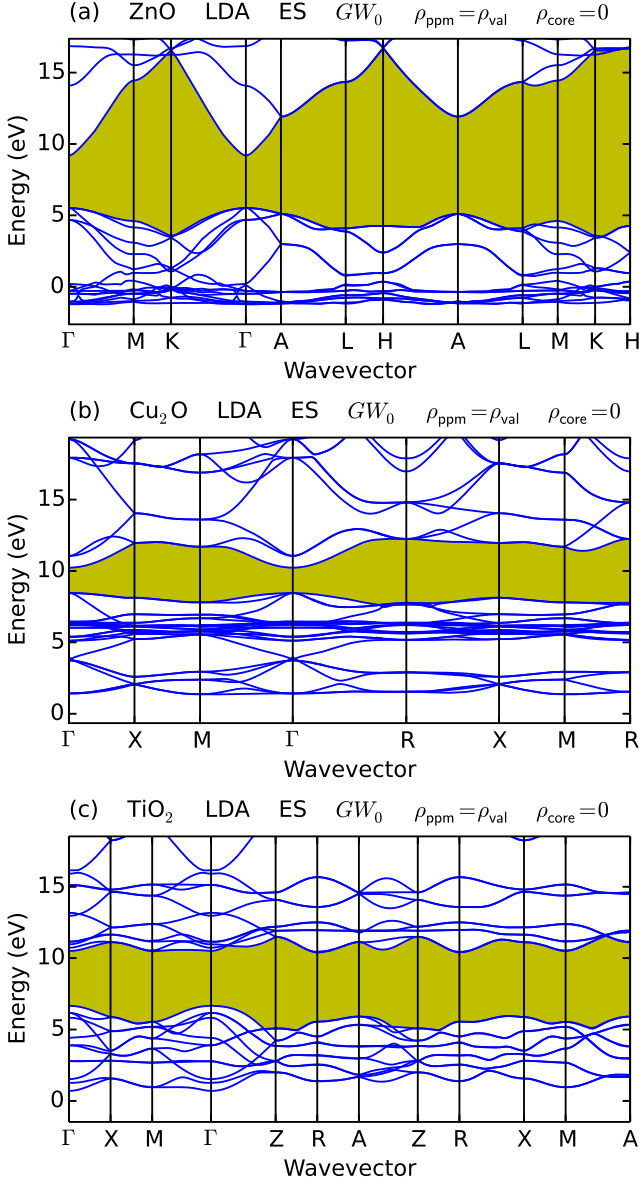


FIG. 2. Quasiparticle band structures of (a) wurtzite ZnO, (b) cuprite Cu₂O, and (c) rutile TiO₂ calculated using the LDA starting point, experimental structural parameters (ES), the eigenvalue self-consistent GW_0 scheme, the HL PPM with $\rho_{\text{ppm}} = \rho_{\text{val}}$, and matrix elements of V_{xc} without NLCC ($\rho_{\text{core}} = 0$). The zero reference for the energy scale is the average ($\mathbf{G} = \mathbf{0}$ component) electrostatic (ionic plus Hartree) potential. The \mathbf{k} -point labeling is from Ref. 58. The band gaps are shaded in yellow.

are carried out for the spin-unpolarized case with the local density approximation (LDA) in the PW form [60] and the generalized gradient approximation (GGA) in the PBE form [61] for the exchange-correlation functional. Norm-conserving pseudopotentials are generated in a separable non-local form [62] using the RRKJ scheme [63] and including scalar relativistic corrections and non-linear core corrections (NLCC) [34]. The pseudopoten-

tial parameters are summarized in Table I. Convergence studies with respect to the size of the Monkhorst-Pack grid [54], kinetic energy cutoffs, and the number of unoccupied Kohn-Sham bands used in the calculation of ϵ and Σ are reported elsewhere [17, 18, 21, 64, 65]. The parameters used in our calculations are summarized in Table II. The Monkhorst-Pack grids for ρ_{scf} , ρ_{val} , and Σ are Γ -centered and the ones for ϵ are shifted by half a grid spacing in all directions. A small wave vector along the (111) direction in crystal coordinates is used to calculate ϵ at the Γ point. The convergence of Σ with respect to the size of the Monkhorst-Pack grid is accelerated by averaging v and W inside the Voronoi cells of the $(\mathbf{k} + \mathbf{G})$ -points near the Γ -point [30]. The convergence of Σ with respect to the number of unoccupied Kohn-Sham bands is accelerated by using the static remainder correction [64]. To ensure convergence of the stress tensor, structural relaxations are performed using 3 times higher kinetic energy cutoffs than those listed in Table II. The experimental and theoretical structural parameters (thereafter referred to as ES and TS, respectively) are listed in Table III.

Special consideration is required when constructing ρ_{val} used in the HL PPM. Given the two formula units per primitive cell and the electronic valence configurations listed in Table I, ZnO, Cu₂O, and TiO₂ have 26, 44, and 24 valence bands, respectively. The top of the valence manifold is derived from the oxygen 2p⁶ states: bands 21–26 in ZnO, bands 39–44 in Cu₂O, and bands 13–24 in TiO₂. The lower valence bands are derived from the oxygen 2s² states and the transition metal third shell: bands 1–20 from O 2s² & Zn 3s²3p⁶3d¹⁰ in ZnO, bands 1–38 from O 2s² & Cu 3s²3p⁶3d¹⁰ in Cu₂O, and bands 1–12 from O 2s² & Ti 3s²3p⁶ in TiO₂. In TiO₂ the oxygen 2p states are separated from the transition metal 3d states by an energy gap, while in ZnO and Cu₂O they overlap. These overlapping states should be decoupled in order to unambiguously construct ρ_{val} from the oxygen 2p⁶ states. For that purpose we employ the DFT+U method with the following parameters: $U = 8.0$ eV and $J = 0.9$ eV for ZnO [17]; $U = 7.5$ eV and $J = 0.98$ eV for Cu₂O [66]. Note that the DFT+U method is only used for constructing ρ_{val} , while GW calculations are carried out starting from DFT orbitals. To quantify the effect of U , we perform two sets of GW calculations, one using DFT ρ_{val} and another using DFT+U ρ_{val} . It is found that the inclusion of U in ρ_{val} only changes the GW band gaps by 10 meV and the GW band edges by 40 meV. The much larger effect of using ρ_{scf} in the HL PPM will be discussed in Sec. IV.

Let us now describe the implementation of the eigenvalue self-consistent GW_0 scheme. Iterations on $E_{n\mathbf{k}}^{\text{QP}}$ entering Eq. (2) are performed by explicitly calculating the matrix elements of Σ and the values of $E_{n\mathbf{k}}^{\text{QP}}$ for several valence and conduction bands near the band edges (16 valence and 14 conduction for ZnO, 26 valence and 10 conduction for Cu₂O, 12 valence and 16 conduction for TiO₂) and by applying the \mathbf{k} -dependent scissors opera-

TABLE IV. Band gaps of wurtzite ZnO measured using photoluminescence (PL) [67] and calculated using DFT and GW. DFT and GW band gaps are obtained using different exchange-correlation functionals (LDA and GGA), experimental and theoretical structural parameters (ES and TS), non-self-consistent G_0W_0 and eigenvalue self-consistent GW_0 schemes, HL PPM with $\rho_{\text{ppm}} = \rho_{\text{val}}$ and ρ_{scf} , and matrix elements of V_{xc} without and with NLCC ($\rho_{\text{core}} = 0$ and $\neq 0$). The DFT and GW band gaps are direct at the Γ point. All values are in eV.

Wurtzite ZnO			LDA		GGA	
	ρ_{ppm}	ρ_{core}	ES	TS	ES	TS
PL ^a				3.44		
DFT			0.74	0.80	0.85	0.78
G_0W_0	ρ_{val}	= 0	3.21	3.32	2.82	2.70
		$\neq 0$	2.50	2.59	2.33	2.23
	ρ_{scf}	= 0	3.82	3.94	3.38	3.26
		$\neq 0$	3.01	3.09	2.82	2.72
GW_0	ρ_{val}	= 0	3.68	3.81	3.24	3.12
		$\neq 0$	2.81	2.90	2.63	2.54
	ρ_{scf}	= 0	4.13	4.25	3.66	3.54
		$\neq 0$	3.23	3.31	3.04	2.94

^a From Ref. 67.

tors to the lower valence and higher conduction bands. The \mathbf{k} -dependent scissor shifts are obtained from the lowest valence and highest conduction bands for which the matrix elements of Σ and the values of $E_{n\mathbf{k}}^{\text{QP}}$ are explicitly calculated. It is found that performing four iterations is sufficient to converge $E_{n\mathbf{k}}^{\text{QP}}$ to within 10 meV.

IV. RESULTS AND DISCUSSION

GW calculations for wurtzite ZnO, cuprite Cu_2O , and rutile TiO_2 are performed using LDA and GGA starting points, experimental and theoretical structural parameters (ES and TS), non-self-consistent G_0W_0 and eigenvalue self-consistent GW_0 schemes, HL PPM with ρ_{ppm} set to DFT+U ρ_{val} and DFT ρ_{scf} , and matrix elements of V_{xc} without and with NLCC ($\rho_{\text{core}} = 0$ and $\neq 0$). In the latter case, values of integrated partial core charge $q_{\text{core}} = \int d\mathbf{r} \rho_{\text{core}}(\mathbf{r})$ are listed in Table I. Fig. 1 shows the real parts of $\epsilon_{00}^{-1}(\mathbf{0}; \omega)$ for the three TMOs in case of the LDA starting point and experimental structural parameters (ES) calculated within the RPA and constructed using the HL PPM with $\rho_{\text{ppm}} = \rho_{\text{val}}$ and ρ_{scf} . Fig. 2 shows the quasiparticle band structures calculated using the LDA starting point, experimental structural parameters (ES), the eigenvalue self-consistent GW_0 scheme, the HL PPM with $\rho_{\text{ppm}} = \rho_{\text{val}}$, and matrix elements of V_{xc} without NLCC ($\rho_{\text{core}} = 0$). Fig. 3 shows the quasiparticle band gaps plotted as a function of the starting point (obtained from the LDA or GGA calculations) and of the structural parameters (either experimental or the-

TABLE V. Band gaps of cuprite Cu_2O measured using optical absorption spectroscopy (OAS) [68] and calculated using DFT and GW. DFT and GW band gaps are obtained using different exchange-correlation functionals (LDA and GGA), experimental and theoretical structural parameters (ES and TS), non-self-consistent G_0W_0 and eigenvalue self-consistent GW_0 schemes, HL PPM with $\rho_{\text{ppm}} = \rho_{\text{val}}$ and ρ_{scf} , and matrix elements of V_{xc} without and with NLCC ($\rho_{\text{core}} = 0$ and $\neq 0$). The DFT and GW band gaps are direct at the Γ point. All values are in eV.

Cuprite Cu ₂ O			LDA		GGA	
	ρ_{ppm}	ρ_{core}	ES	TS	ES	TS
OAS ^a				2.17		
DFT			0.52	0.69	0.53	0.47
G_0W_0	ρ_{val}	= 0	1.56	1.71	1.51	1.46
		≠ 0	1.14	0.87	0.91	1.01
	ρ_{scf}	= 0	1.76	1.91	1.70	1.65
		≠ 0	1.26	0.97	1.01	1.11
GW_0	ρ_{val}	= 0	1.77	1.92	1.70	1.66
		≠ 0	1.13	0.85	0.90	0.99
	ρ_{scf}	= 0	1.87	2.03	1.80	1.75
		≠ 0	1.32	1.03	1.08	1.18

^a From Ref. 68.

TABLE VI. Band gaps of rutile TiO_2 measured using photoemission spectroscopy (PES) [69] and calculated using DFT and GW. DFT and GW band gaps are obtained using different exchange-correlation functionals (LDA and GGA), experimental and theoretical structural parameters (ES and TS), non-self-consistent G_0W_0 and eigenvalue self-consistent GW_0 schemes, HL PPM with $\rho_{\text{ppm}} = \rho_{\text{val}}$ and ρ_{scf} , and matrix elements of V_{xc} without and with NLCC ($\rho_{\text{core}} = 0$ and $\neq 0$). The DFT and GW band gaps are direct at the Γ point (in regular font) and indirect between the Γ point at the VBM and the R point at the CBM (in cursive font). All values are in eV.

Rutile TiO ₂			LDA		GGA	
	ρ_{ppm}	ρ_{core}	ES	TS	ES	TS
PES ^a				3.60		
DFT			1.82	1.85	1.90	1.85
G_0W_0	ρ_{val}	= 0	3.44	3.53	3.42	3.34
		≠ 0	3.69	3.78	3.65	3.57
	ρ_{scf}	= 0	3.28	3.35	3.23	3.14
		≠ 0	3.57	3.63	3.48	3.41
GW_0	ρ_{val}	= 0	3.72	3.82	3.70	3.61
		≠ 0	4.03	4.12	3.98	3.90
	ρ_{scf}	= 0	3.48	3.56	3.43	3.35
		≠ 0	3.79	3.86	3.70	3.63

^a From Ref. 69.

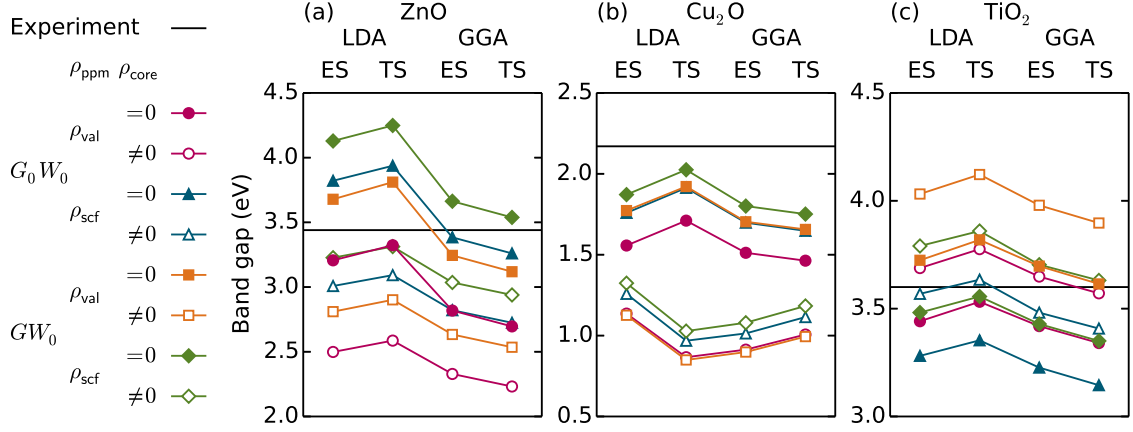


FIG. 3. Quasiparticle band gaps of (a) wurtzite ZnO, (b) cuprite Cu₂O, and (c) rutile TiO₂ calculated within the GW method and plotted as a function of the starting point (obtained from the LDA or GGA calculations) and of the structural parameters (either experimental or theoretical, labeled as ES and TS, respectively). Different symbols indicate the values calculated using different flavors of the GW method, as shown in the legend on the left. The experimental band gaps taken from Refs. 67–69 are shown by horizontal lines.

oretical, labeled as ES and TS, respectively). Different symbols indicate the values calculated using different flavors of the GW method. In this context, flavor refers to the choice of self-consistent scheme, ρ_{ppm} , and ρ_{core} . The experimental band gaps taken from Refs. 67–69 are shown for comparison. Tables IV–VI give the experimental and calculated band gaps plotted in Fig. 3 as well as the Kohn-Sham values not shown in Fig. 3. Kohn-Sham and quasiparticle band energies $E_{n\mathbf{k}}^{\text{KS}}$ and $E_{n\mathbf{k}}^{\text{QP}}$ and matrix elements of V_{xc} and Σ at the valence band maximum (VBM) and conduction band minimum (CBM) are provided in Supplemental Material [70].

Comparing Fig. 1(a) with Fig. 2(a) of Ref. 21, Fig. 5(a) of Ref. 23, and Fig. 4(d) of Ref. 26, we find that in the case of ZnO, the HL PPM becomes similar to the GN PPM when ρ_{ppm} is set to ρ_{val} . One can see from Fig. 1 that for all three oxides, the HL PPM with $\rho_{\text{ppm}} = \rho_{\text{val}}$ gives a better fit to the RPA results than the HL PPM with $\rho_{\text{ppm}} = \rho_{\text{scf}}$. We note that the HL PPM suffers from the ambiguity of constructing the proper ρ_{ppm} . This problem is absent in the GN PPM, suggesting that the HL PPM is more difficult to use for studying TMOs than the GN PPM.

Several conclusions can be drawn from statistical analysis of the data presented in Fig. 3 and Tables IV–VI.

- Comparing the values in $(G_0W_0, \rho_{\text{val}}, 0)$ row at (LDA, ES) and (GGA, ES) columns for ZnO, we find that the band gap varies by $3.21 - 2.82 = 0.39$ eV depending on the starting point (obtained from the LDA or GGA calculations). Averaging this quantity over different $\rho_{\text{core}} = 0$ rows for ZnO gives the mean variation in the band gap with different starting points as equal to 0.44 eV. Repeating this procedure for Cu₂O and TiO₂ yields the values of 0.06 eV and 0.04 eV, respectively. The large variation in the case of ZnO indicates that

neither LDA nor GGA provides a good starting point for GW calculations. At the same time, small variations for Cu₂O and TiO₂ imply that LDA and GGA give similar (but not necessarily good) starting points for GW calculations. Other starting points were tried in GW calculations for ZnO including DFT+U [17], the screened hybrid functional [15], and the exact exchange optimized effective potential [20]. Note that the latter starting point can present some challenges in the subsequent GW calculations [71]. Overall, the problem of the starting point in GW calculations for ZnO may require further research to give the full picture.

- Comparison of the values in $\rho_{\text{core}} = 0$ rows at (LDA, ES) and (LDA, TS) columns, as well as at (GGA, ES) and (GGA, TS) columns, shows that the variation of the band gap with the structural parameters is 0.12 eV for ZnO, 0.10 eV for Cu₂O, and 0.09 eV for TiO₂. This suggests that the band gaps are fairly insensitive to the structural parameters.
- Comparing the values in $(G_0W_0, \rho_{\text{val}}, 0)$ and $(GW_0, \rho_{\text{val}}, 0)$ rows, as well as in $(G_0W_0, \rho_{\text{scf}}, 0)$ and $(GW_0, \rho_{\text{scf}}, 0)$ rows, we find that the eigenvalue self-consistency in G increases the band gap by 0.37 eV for ZnO, 0.16 eV for Cu₂O, and 0.24 eV for TiO₂. This is consistent with previous studies [13].
- Comparison of the values in $(G_0W_0, \rho_{\text{val}}, 0)$ and $(G_0W_0, \rho_{\text{scf}}, 0)$ rows, as well as in $(GW_0, \rho_{\text{val}}, 0)$ and $(GW_0, \rho_{\text{scf}}, 0)$ rows, shows that the inclusion of core electrons in ρ_{ppm} increases the band gap of ZnO and Cu₂O by 0.51 and 0.15 eV, respectively, and decreases the band gap of TiO₂ by 0.22 eV. This is because for ZnO and Cu₂O, the VBM is

lowered by a larger amount than the CBM, while the opposite scenario takes place for TiO_2 , as follows from Supplemental Material [70].

- Comparing the values in $\rho_{\text{core}} = 0$ and $\rho_{\text{core}} \neq 0$ rows, we find that the inclusion of NLCC in the matrix elements of V_{xc} decreases the band gap of ZnO and Cu_2O by 0.70 and 0.69 eV, respectively, and increases the band gap of TiO_2 by 0.27 eV. This is due to the fact that for ZnO and Cu_2O , the VBM is raised by a larger amount than the CBM, while the opposite holds for TiO_2 , as one can see from Supplemental Material [70].

Overall, the largest variation of the band gap comes from the inclusion of NLCC in the matrix elements of V_{xc} . This inclusion introduces significant errors in the calculated band gaps.

Fair agreement is found when comparing our results to those of previous GW calculations for each oxide and specific flavor. In line with the criticism of the HL PPM [21, 23, 26], previous HL PPM calculations are compared to our $\rho_{\text{ppm}} = \rho_{\text{scf}}$ results, while previous GN PPM and non-PPM calculations to our $\rho_{\text{ppm}} = \rho_{\text{val}}$ results.

- For ZnO, we focus on (LDA, ES) column in Fig. 3(a) or Table IV. The most accurate non-PPM G_0W_0 calculations gave the following values for the band gap: 2.83 eV with the full potential linearized augmented plane wave (FLAPW) method [18] and 2.87 eV with the projector augmented wave (PAW) method [27]. We find that the HL PPM gives a somewhat larger value of 3.21 eV and a substantially larger value of 3.82 eV when ρ_{ppm} is set to ρ_{val} and ρ_{scf} , respectively. Previous HL PPM G_0W_0 calculations showed values in this range, 3.4 eV [17], 3.57 eV [21], and 3.56 eV [23], with one exception where the value of 2.80 eV was reported [26]. Other studies reported much lower values, such as non-PPM G_0W_0 band gaps of 2.17–2.43 eV [23, 26] and the GN PPM G_0W_0 band gaps of 2.27–2.56 eV [21–23, 26]. We do not compare to the results of Refs. [12–14, 16, 25] which may be affected by the basis set convergence issues as discussed in Ref. 27.
- For Cu_2O , let us look at (LDA, ES) column in Fig. 3(b) or Table V. The $(G_0W_0, \rho_{\text{val}}, 0)$ band gap of 1.56 eV compares with non-PPM G_0W_0 value of 1.34 eV [72]. The $(GW_0, \rho_{\text{val}}, 0)$ band gap of 1.77 eV is close to non-PPM eigenvalue self-consistent GW band gap of 1.80 eV [72].
- For TiO_2 , we start with (LDA, ES) column in Fig. 3(c) or Table VI. The $(G_0W_0, \rho_{\text{val}}, 0)$ band gap of 3.44 eV is close to non-PPM G_0W_0 value of 3.34 eV [38]. We now move on to (GGA, TS) column. The $(G_0W_0, \rho_{\text{val}}, 0)$ band gap of 3.34 eV is comparable to the GN PPM G_0W_0 value of 3.59 eV [73]. The $(G_0W_0, \rho_{\text{scf}}, 0)$ band gap of 3.14 eV is close to the HL PPM G_0W_0 value of 3.13 eV [65].

We now compare the calculated band gaps with the experimental data. The absolute difference of the experimental band gap and the value in $(G_0W_0, \rho_{\text{val}}, 0)$ row at (LDA, ES) column for ZnO is equal to 0.23 eV. Averaging this quantity over the four columns in Fig. 3(a) or Table IV gives the value of 0.43 eV. Further averaging over the three TMOs gives the mean deviation from experiment of 0.40 eV. This procedure is repeated for each flavor represented by different row in Fig. 3 and Tables IV–VI. Among the eight flavors, the smallest deviation of 0.18 eV is found for $(GW_0, \rho_{\text{val}}, 0)$ flavor, followed by the 0.30 eV deviation for $(GW_0, \rho_{\text{scf}}, 0)$ flavor, the 0.31 eV deviation for $(G_0W_0, \rho_{\text{scf}}, 0)$ flavor, and the 0.40 eV deviation for $(G_0W_0, \rho_{\text{val}}, 0)$ flavor. Corresponding deviations for $\rho_{\text{core}} \neq 0$ rows fall within the 0.49 to 0.78 eV range. We conclude that the best overall agreement with experiment is obtained for $(GW_0, \rho_{\text{val}}, 0)$ flavor. On the other hand, we note from Fig. 3 that $(GW_0, \rho_{\text{val}}, 0)$ values irregularly underestimate and overestimate the experimental band gaps, while $(G_0W_0, \rho_{\text{val}}, 0)$ values always underestimate the experiment, suggesting that the latter flavor may be preferable to the former. Yet this conclusion may be deceiving given that the HL PPM with ρ_{val} overestimates the non-PPM band gap of ZnO by 0.34–0.38 eV (see the comparison with the previous calculations above) and that the experimental band gaps are renormalized by electron-phonon interaction not included in our calculations. Overall, it may be premature to conclude which flavor is preferable for TMOs until the effect of the vertex correction on GW band gaps of these materials is thoroughly studied.

V. SUMMARY

In summary, we quantify the effects of different approximations used in the GW method on the band gaps and band edges for three TMOs: wurtzite ZnO, cuprite Cu_2O , and rutile TiO_2 . It is found that the GW band gap of ZnO is sensitive to the starting point obtained from the LDA or GGA calculations, suggesting that the Kohn-Sham orbitals differ from the quasiparticle orbitals. It is shown that the HL PPM becomes similar to the GN PPM and gives better agreement with the RPA when ρ_{ppm} is set to ρ_{val} , that is, only the valence electrons are used to determine the effective bare plasma frequencies for the HL PPM. It is demonstrated that the theoretically justified choice of approximations, namely eigenvalue self-consistent GW_0 scheme, ρ_{val} in the HL PPM, and the proper treatment of the V_{xc} term, give the best overall agreement between the calculated and measured band gaps.

ACKNOWLEDGMENTS

We are grateful to Dr. Brad D. Malone for implementing the $\rho_{\text{ppm}} = \rho_{\text{val}}$ option in the Quantum ESPRESSO

interface to **BerkeleyGW**. We thank Mr. Felipe H. Jornada for implementing the Delaunay tessellation for band structure interpolation in **BerkeleyGW**. We acknowledge helpful comments on an early version of the paper by Prof. Peihong Zhang, Prof. Gian-Marco Rignanese, and Mr. Derek Vigil. G.S. and B.K. acknowledge support from DOE (Grant No. DE-EE0004840) and NSF (Grant

No. 1048796), C.H.P. from Korean NRF funded by MSIP (Grant No. NRF-2013R1A1A1076141). This research used resources of the Oak Ridge Leadership Computing Facility located in the Oak Ridge National Laboratory, which is supported by the Office of Science of the Department of Energy under Contract DE-AC05-00OR22725.

-
- [1] L. Hedin, *Phys. Rev.* **139**, A796 (1965).
 - [2] L. Hedin and S. Lundqvist, *Solid State Phys.* **23**, 1 (1970).
 - [3] G. Strinati, H. J. Mattausch, and W. Hanke, *Phys. Rev. Lett.* **45**, 290 (1980).
 - [4] G. Strinati, H. J. Mattausch, and W. Hanke, *Phys. Rev. B* **25**, 2867 (1982).
 - [5] M. S. Hybertsen and S. G. Louie, *Phys. Rev. Lett.* **55**, 1418 (1985).
 - [6] R. W. Godby, M. Schlüter, and L. J. Sham, *Phys. Rev. Lett.* **56**, 2415 (1986).
 - [7] M. S. Hybertsen and S. G. Louie, *Phys. Rev. B* **34**, 5390 (1986).
 - [8] R. W. Godby, M. Schlüter, and L. J. Sham, *Phys. Rev. B* **37**, 10159 (1988).
 - [9] F. Aryasetiawan and O. Gunnarsson, *Rep. Prog. Phys.* **61**, 237 (1998).
 - [10] G. Onida, L. Reining, and A. Rubio, *Rev. Mod. Phys.* **74**, 601 (2002).
 - [11] M. Usuda, N. Hamada, T. Kotani, and M. van Schilf-gaarde, *Phys. Rev. B* **66**, 125101 (2002).
 - [12] T. Kotani, M. van Schilf-gaarde, and S. V. Faleev, *Phys. Rev. B* **76**, 165106 (2007).
 - [13] M. Shishkin and G. Kresse, *Phys. Rev. B* **75**, 235102 (2007).
 - [14] F. Fuchs, J. Furthmüller, F. Bechstedt, M. Shishkin, and G. Kresse, *Phys. Rev. B* **76**, 115109 (2007).
 - [15] A. Schleife, C. Rödl, F. Fuchs, J. Furthmüller, F. Bechstedt, P. H. Jefferson, T. D. Veal, C. F. McConville, L. F. J. Piper, A. DeMasi, K. E. Smith, H. Lösch, R. Goldhahn, C. Cobet, J. Zúñiga-Pérez, and V. Muñoz-Sanjósé, *J. Korean Phys. Soc.* **53**, 2811 (2008).
 - [16] F. Bechstedt, F. Fuchs, and G. Kresse, *Phys. Status Solidi B* **246**, 1877 (2009).
 - [17] B.-C. Shih, Y. Xue, P. Zhang, M. L. Cohen, and S. G. Louie, *Phys. Rev. Lett.* **105**, 146401 (2010).
 - [18] C. Friedrich, M. C. Müller, and S. Blügel, *Phys. Rev. B* **83**, 081101 (2011).
 - [19] H. Dixit, R. Saniz, D. Lamoén, and B. Partoens, *Comput. Phys. Commun.* **182**, 2029 (2011).
 - [20] Q. Yan, P. Rinke, M. Winkelnkemper, A. Qteish, D. Bimberg, M. Scheffler, and C. G. V. de Walle, *Semicond. Sci. Technol.* **26**, 014037 (2011).
 - [21] M. Stankovski, G. Antonius, D. Waroquiers, A. Miglio, H. Dixit, K. Sankaran, M. Giantomassi, X. Gonze, M. Côté, and G.-M. Rignanese, *Phys. Rev. B* **84**, 241201 (2011).
 - [22] J. A. Berger, L. Reining, and F. Sottile, *Phys. Rev. B* **85**, 085126 (2012).
 - [23] A. Miglio, D. Waroquiers, G. Antonius, M. Giantomassi, M. Stankovski, M. Côté, X. Gonze, and G.-M. Rignanese, *Eur. Phys. J. B* **85**, 322 (2012).
 - [24] S. Lany, *Phys. Rev. B* **87**, 085112 (2013).
 - [25] F. Hüsler, T. Olsen, and K. S. Thygesen, *Phys. Rev. B* **87**, 235132 (2013).
 - [26] P. Larson, M. Dvorak, and Z. Wu, *Phys. Rev. B* **88**, 125205 (2013).
 - [27] J. Klimeš, M. Kaltak, and G. Kresse, *Phys. Rev. B* **90**, 075125 (2014).
 - [28] M. van Schilf-gaarde, T. Kotani, and S. Faleev, *Phys. Rev. Lett.* **96**, 226402 (2006).
 - [29] F. Bruneval, N. Vast, and L. Reining, *Phys. Rev. B* **74**, 045102 (2006).
 - [30] J. Deslippe, G. Samsonidze, D. A. Strubbe, M. Jain, M. L. Cohen, and S. G. Louie, *Comput. Phys. Commun.* **183**, 1269 (2012).
 - [31] X.-Z. Li, R. Gómez-Abal, H. Jiang, C. Ambrosch-Draxl, and M. Scheffler, *New J. Phys.* **14**, 023006 (2012).
 - [32] W. Kohn and L. J. Sham, *Phys. Rev.* **140**, A1133 (1965).
 - [33] D. R. Hamann, M. Schlüter, and C. Chiang, *Phys. Rev. Lett.* **43**, 1494 (1979).
 - [34] S. G. Louie, S. Froyen, and M. L. Cohen, *Phys. Rev. B* **26**, 1738 (1982).
 - [35] M. Rohlfing, P. Krüger, and J. Pollmann, *Phys. Rev. Lett.* **75**, 3489 (1995).
 - [36] M. Rohlfing, P. Krüger, and J. Pollmann, *Phys. Rev. B* **56**, R7065 (1997).
 - [37] A. Marini, G. Onida, and R. Del Sole, *Phys. Rev. Lett.* **88**, 016403 (2001).
 - [38] W. Kang and M. S. Hybertsen, *Phys. Rev. B* **82**, 085203 (2010).
 - [39] P. Umari and S. Fabris, *The Journal of Chemical Physics* **136**, 174310 (2012).
 - [40] B. Arnaud and M. Alouani, *Phys. Rev. B* **62**, 4464 (2000).
 - [41] A. Fleszar and W. Hanke, *Phys. Rev. B* **71**, 045207 (2005).
 - [42] R. Gómez-Abal, X. Li, M. Scheffler, and C. Ambrosch-Draxl, *Phys. Rev. Lett.* **101**, 106404 (2008).
 - [43] S. V. Faleev, M. van Schilf-gaarde, and T. Kotani, *Phys. Rev. Lett.* **93**, 126406 (2004).
 - [44] W.-D. Schöne and A. G. Eguiluz, *Phys. Rev. Lett.* **81**, 1662 (1998).
 - [45] E. L. Shirley, *Phys. Rev. B* **54**, 7758 (1996).
 - [46] U. von Barth and B. Holm, *Phys. Rev. B* **54**, 8411 (1996).
 - [47] B. Holm and U. von Barth, *Phys. Rev. B* **57**, 2108 (1998).
 - [48] Y. Takada, *Phys. Rev. Lett.* **87**, 226402 (2001).
 - [49] M. Shishkin and G. Kresse, *Phys. Rev. B* **74**, 035101 (2006).
 - [50] S. Lebègue, B. Arnaud, M. Alouani, and P. E. Blochl, *Phys. Rev. B* **67**, 155208 (2003).
 - [51] S. B. Zhang, D. Tománek, M. L. Cohen, S. G. Louie, and M. S. Hybertsen, *Phys. Rev. B* **40**, 3162 (1989).
 - [52] R. W. Godby and R. J. Needs, *Phys. Rev. Lett.* **62**, 1169 (1989).

- [53] A. Kaur, E. R. Ylvisaker, D. Lu, T. A. Pham, G. Galli, and W. E. Pickett, *Phys. Rev. B* **87**, 155144 (2013).
- [54] H. J. Monkhorst and J. D. Pack, *Phys. Rev. B* **13**, 5188 (1976).
- [55] K. Kihara and G. Donnay, *Can. Mineral.* **23**, 647 (1985).
- [56] A. Kirfel and K. Eichhorn, *Acta Crystallogr. A* **46**, 271 (1990).
- [57] S. C. Abrahams and J. L. Bernstein, *J. Chem. Phys.* **55**, 3206 (1971).
- [58] W. Setyawan and S. Curtarolo, *Comp. Mater. Sci.* **49**, 299 (2010).
- [59] P. Giannozzi, S. Baroni, N. Bonini, M. Calandra, R. Car, C. Cavazzoni, D. Ceresoli, G. L. Chiarotti, M. Cococcioni, I. Dabo, A. D. Corso, S. de Gironcoli, S. Fabris, G. Fratesi, R. Gebauer, U. Gerstmann, C. Gougoussis, A. Kokalj, M. Lazzeri, L. Martin-Samos, N. Marzari, F. Mauri, R. Mazzarello, S. Paolini, A. Pasquarello, L. Paulatto, C. Sbraccia, S. Scandolo, G. Sclauzero, A. P. Seitsonen, A. Smogunov, P. Umari, and R. M. Wentzcovitch, *J. Phys.: Condens. Matter* **21**, 395502 (2009).
- [60] J. P. Perdew and Y. Wang, *Phys. Rev. B* **45**, 13244 (1992).
- [61] J. P. Perdew, K. Burke, and M. Ernzerhof, *Phys. Rev. Lett.* **77**, 3865 (1996).
- [62] L. Kleinman and D. M. Bylander, *Phys. Rev. Lett.* **48**, 1425 (1982).
- [63] A. M. Rappe, K. M. Rabe, E. Kaxiras, and J. D. Joannopoulos, *Phys. Rev. B* **41**, 1227 (1990).
- [64] J. Deslippe, G. Samsonidze, M. Jain, M. L. Cohen, and S. G. Louie, *Phys. Rev. B* **87**, 165124 (2013).
- [65] A. Malashevich, M. Jain, and S. G. Louie, *Phys. Rev. B* **89**, 075205 (2014).
- [66] M. Heinemann, B. Eifert, and C. Heiliger, *Phys. Rev. B* **87**, 115111 (2013).
- [67] D. C. Reynolds, D. C. Look, B. Jogai, C. W. Litton, G. Cantwell, and W. C. Harsch, *Phys. Rev. B* **60**, 2340 (1999).
- [68] P. W. Baumeister, *Phys. Rev.* **121**, 359 (1961).
- [69] S. Rangan, S. Katalinic, R. Thorpe, R. A. Bartynski, J. Rochford, and E. Galoppini, *J. Phys. Chem. C* **114**, 1139 (2010).
- [70] See Supplemental Material for E_{nk}^{KS} and E_{nk}^{QP} and matrix elements of V_{xc} and Σ at the VBM and CBM of ZnO, Cu₂O, and TiO₂.
- [71] A. Fleszar, *Phys. Rev. B* **64**, 245204 (2001).
- [72] F. Bruneval, N. Vast, L. Reining, M. Izquierdo, F. Sirotti, and N. Barrett, *Phys. Rev. Lett.* **97**, 267601 (2006).
- [73] L. Chiodo, J. M. García-Lastra, A. Iacomino, S. Ossicini, J. Zhao, H. Petek, and A. Rubio, *Phys. Rev. B* **82**, 045207 (2010).

Supplemental material: Insights and challenges of applying the GW method to transition metal oxides

Georgy Samsonidze,¹ Cheol-Hwan Park,² and Boris Kozinsky¹

¹*Research and Technology Center, Robert Bosch LLC, Cambridge, Massachusetts 02142, USA*

²*Department of Physics, Seoul National University, Seoul 151-747, Korea*

(Dated: October 31, 2014)

TABLE I. Kohn-Sham and quasiparticle energies (E^{KS} and E^{QP}) and matrix elements of V_{xc} and Σ at the valence band maximum (VBM) and conduction band minimum (CBM) of wurtzite ZnO calculated within DFT and GW using different exchange-correlation functionals (LDA and GGA), experimental and theoretical structural parameters (ES and TS), non-self-consistent G_0W_0 and eigenvalue self-consistent GW_0 schemes, HL PPM with $\rho_{\text{ppm}} = \rho_{\text{val}}$ and ρ_{scf} , and matrix elements of V_{xc} without and with NLCC ($\rho_{\text{core}} = 0$ and $\neq 0$). The VBM and CBM are at the Γ point. All values are in eV. The zero reference for the energy scale is the average ($\mathbf{G} = \mathbf{0}$ component) electrostatic (ionic plus Hartree) potential.

Wurtzite ZnO			LDA				GGA			
			ES		TS		ES		TS	
	ρ_{ppm}	ρ_{core}	VBM	CBM	VBM	CBM	VBM	CBM	VBM	CBM
DFT		E^{KS}	7.88	8.63	8.62	9.43	8.34	9.19	7.72	8.50
		V_{xc}	-26.66	-13.35	-27.13	-13.51	-27.06	-12.77	-26.52	-12.58
		$\neq 0$	-28.02	-13.76	-28.54	-13.92	-27.98	-13.04	-27.42	-12.85
		E^{QP}	6.00	9.21	6.70	10.02	6.63	9.45	6.05	8.74
G_0W_0	ρ_{val}	Σ	-28.54	-12.77	-29.06	-12.91	-28.77	-12.52	-28.20	-12.34
		E^{QP}	7.04	9.54	7.77	10.36	7.34	9.67	6.73	8.96
		Σ	-28.86	-12.85	-29.39	-12.98	-28.98	-12.56	-28.41	-12.39
		E^{QP}	4.85	8.67	5.55	9.48	5.51	8.89	4.93	8.19
GW_0	ρ_{scf}	Σ	-29.69	-13.31	-30.21	-13.45	-29.88	-13.07	-29.31	-12.89
		E^{QP}	6.03	9.04	6.77	9.86	6.32	9.14	5.71	8.43
		Σ	-29.87	-13.35	-30.40	-13.49	-30.01	-13.10	-29.43	-12.92
		E^{QP}	5.53	9.21	6.22	10.03	6.16	9.41	5.58	8.70
GW_0	ρ_{val}	Σ	-29.01	-12.77	-29.54	-12.90	-29.23	-12.56	-28.66	-12.39
		E^{QP}	6.85	9.66	7.58	10.49	7.07	9.71	6.46	9.00
		Σ	-29.05	-12.73	-29.58	-12.86	-29.25	-12.52	-28.68	-12.35
		E^{QP}	4.48	8.61	5.18	9.43	5.15	8.81	4.57	8.11
GW_0	ρ_{scf}	Σ	-30.06	-13.37	-30.58	-13.50	-30.25	-13.15	-29.67	-12.98
		E^{QP}	5.82	9.05	6.56	9.87	6.06	9.10	5.45	8.39
		Σ	-30.08	-13.34	-30.60	-13.48	-30.26	-13.13	-29.69	-12.96
		E^{QP}								

TABLE II. Kohn-Sham and quasiparticle energies (E^{KS} and E^{QP}) and matrix elements of V_{xc} and Σ at the valence band maximum (VBM) and conduction band minimum (CBM) of cuprite Cu_2O calculated within DFT and GW using different exchange-correlation functionals (LDA and GGA), experimental and theoretical structural parameters (ES and TS), non-self-consistent G_0W_0 and eigenvalue self-consistent GW_0 schemes, HL PPM with $\rho_{\text{ppm}} = \rho_{\text{val}}$ and ρ_{scf} , and matrix elements of V_{xc} without and with NLCC ($\rho_{\text{core}} = 0$ and $\neq 0$). The VBM and CBM are at the Γ point. All values are in eV. The zero reference for the energy scale is the average ($\mathbf{G} = \mathbf{0}$ component) electrostatic (ionic plus Hartree) potential.

Cuprite Cu_2O			LDA				GGA			
			ES		TS		ES		TS	
	ρ_{ppm}	ρ_{core}	VBM	CBM	VBM	CBM	VBM	CBM	VBM	CBM
DFT		E^{KS}	9.52	10.04	10.67	11.36	9.99	10.52	9.60	10.07
		V_{xc}	-32.10	-30.69	-32.24	-30.86	-32.40	-30.95	-32.35	-30.88
		E^{QP}	8.73	10.29	9.89	11.60	9.37	10.88	8.97	10.43
		Σ	-32.89	-30.44	-33.02	-30.62	-33.03	-30.58	-32.98	-30.52
G_0W_0	ρ_{val}	E^{QP}	10.04	11.18	11.22	12.09	10.34	11.25	9.93	10.94
		Σ	-33.44	-31.35	-33.57	-31.95	-33.44	-31.56	-33.39	-31.35
		E^{QP}	7.67	9.43	8.83	10.75	8.35	10.05	7.94	9.59
		Σ	-33.95	-31.30	-34.07	-31.47	-34.05	-31.42	-34.00	-31.36
GW_0	ρ_{scf}	E^{QP}	9.24	10.50	10.43	11.39	9.51	10.52	9.10	10.22
		Σ	-34.24	-32.03	-34.37	-32.65	-34.27	-32.28	-34.22	-32.07
		E^{QP}	8.46	10.23	9.63	11.55	9.12	10.83	8.72	10.37
		Σ	-33.16	-30.50	-33.28	-30.67	-33.27	-30.64	-33.23	-30.57
	ρ_{val}	E^{QP}	10.21	11.34	11.40	12.25	10.42	11.32	10.01	11.01
		Σ	-33.27	-31.19	-33.39	-31.79	-33.35	-31.48	-33.31	-31.28
		E^{QP}	7.37	9.24	8.54	10.57	8.06	9.86	7.65	9.40
		Σ	-34.25	-31.49	-34.36	-31.65	-34.33	-31.60	-34.29	-31.54
	ρ_{scf}	E^{QP}	9.17	10.50	10.36	11.39	9.39	10.47	8.98	10.16
		Σ	-34.31	-32.03	-34.43	-32.65	-34.38	-32.33	-34.34	-32.12

TABLE III. Kohn-Sham and quasiparticle energies (E^{KS} and E^{QP}) and matrix elements of V_{xc} and Σ at the valence band maximum (VBM) and conduction band minimum (CBM) of rutile TiO_2 calculated within DFT and GW using different exchange-correlation functionals (LDA and GGA), experimental and theoretical structural parameters (ES and TS), non-self-consistent G_0W_0 and eigenvalue self-consistent GW_0 schemes, HL PPM with $\rho_{\text{ppm}} = \rho_{\text{val}}$ and ρ_{scf} , and matrix elements of V_{xc} without and with NLCC ($\rho_{\text{core}} = 0$ and $\neq 0$). The VBM and CBM are at the Γ point (in regular font) and at the R point (in cursive font). All values are in eV. The zero reference for the energy scale is the average ($\mathbf{G} = \mathbf{0}$ component) electrostatic (ionic plus Hartree) potential.

Rutile TiO ₂			LDA				GGA				
			ES		TS		ES		TS		
	ρ_{ppm}	ρ_{core}	VBM	CBM	VBM	CBM	VBM	CBM	VBM	CBM	
DFT		E^{KS}	8.07	9.88	8.45	10.30	8.43	10.33	8.00	9.84	
		$= 0$	V_{xc}	-20.29	-20.31	-20.36	-20.33	-20.56	-20.36	-20.48	-20.36
		$\neq 0$		-21.12	-21.44	-21.19	-21.45	-21.04	-21.14	-20.97	-21.14
G_0W_0	ρ_{val}	$= 0$	E^{QP}	6.90	<i>10.34</i>	7.27	<i>10.80</i>	7.42	<i>10.84</i>	7.00	<i>10.35</i>
			Σ	-21.46	-19.38	-21.54	-19.35	-21.57	-19.39	-21.48	-19.38
		$\neq 0$	E^{QP}	7.55	<i>11.23</i>	7.92	<i>11.69</i>	7.79	<i>11.44</i>	7.38	<i>10.95</i>
	ρ_{scf}		Σ	-21.64	-19.58	-21.73	-19.54	-21.68	-19.54	-21.59	-19.53
		$= 0$	E^{QP}	6.58	<i>9.87</i>	6.96	<i>10.31</i>	7.11	<i>10.34</i>	6.69	9.84
			Σ	-21.77	-19.86	-21.85	-19.83	-21.88	-19.89	-21.79	-20.36
GW_0	ρ_{val}	$\neq 0$	E^{QP}	7.26	<i>10.83</i>	7.64	<i>11.27</i>	7.51	<i>10.99</i>	7.09	10.50
			Σ	-21.93	-19.98	-22.00	-19.96	-21.97	-19.99	-21.88	-20.48
		$= 0$	E^{QP}	6.66	<i>10.39</i>	7.03	<i>10.85</i>	7.19	<i>10.88</i>	6.77	<i>10.39</i>
	ρ_{scf}		Σ	-21.69	-19.33	-21.78	-19.30	-21.80	-19.34	-21.71	-19.33
		$\neq 0$	E^{QP}	7.48	<i>11.51</i>	7.85	<i>11.97</i>	7.67	<i>11.65</i>	7.26	<i>11.15</i>
			Σ	-21.71	-19.30	-21.79	-19.26	-21.80	-19.33	-21.71	-19.33
	ρ_{scf}	$= 0$	E^{QP}	6.33	<i>9.81</i>	6.70	<i>10.26</i>	6.86	<i>10.29</i>	6.44	9.80
			Σ	-22.03	-19.91	-22.10	-19.89	-22.13	-19.93	-22.04	-20.40
		$\neq 0$	E^{QP}	7.15	<i>10.94</i>	7.53	<i>11.38</i>	7.34	<i>11.05</i>	6.93	<i>10.56</i>
		Σ	-22.04	-19.87	-22.12	-19.85	-22.13	-19.93	-22.04	-19.92	